EUROPEAN ORGANIZATION FOR NUCLEAR RESEARCH

Measurement of the Electron Structure Function at LEP energies

DELPHI Collaboration

Abstract

The hadronic part of the Electron Structure Function (ESF) has been measured for the first time, using e^+e^- data collected by the DELPHI experiment at LEP, at centre-of-mass energies $\sqrt{s} = 91.2 - 209.5$ GeV. The data analysis is simpler than that of the measurement of the photon structure function. The ESF data are compared to predictions of phenomenological models based on the photon structure function. It is shown that the quasi-real photon virtuality contribution is significant. The presented data can serve as a cross-check of the photon structure function analyses and help in refining existing parametrizations.

CERN-PH-EP-2010-058
09/11/2010

(Submitted to Phys. Lett. B)

J.Abdallah[28], P.Abreu[25], W.Adam[57], P.Adzic[13], T.Albrecht[19], R.Alemany-Fernandez[10], T.Allmendinger[19], P.P.Allport[26], U.Amaldi[32], N.Amapane[50], S.Amato[54], E.Anashkin[39], A.Andreazza[31], S.Andringa[25], N.Anjos[25], P.Antilogus[28], W-D.Apel[19], Y.Arnoud[16], S.Ask[10], B.Asman[49], J.E.Augustin[28], A.Augustinus[10], P.Baillon[10], A.Ballestrero[51], P.Bambade[23], R.Barbier[30], D.Bardin[18], G.J.Barker[59], A.Baroncelli[42], M.Battaglia[10], M.Baubillier[28], K-H.Becks[60], M.Begalli[8], A.Behrmann[60], E.Ben-Haim[28], N.Benekos[35], A.Benvenuti[6], C.Berat[16], M.Berggren[28], D.Bertrand[3], M.Besancon[43], N.Besson[43], D.Bloch[11], M.Blom[34], M.Bluj[58], M.Bonesini[32], M.Boonekamp[43], P.S.L.Booth†[26], G.Borisov[24], O.Botner[55], B.Bouquet[23], T.J.V.Bowcock[26], I.Boyko[18], M.Bracko[46], R.Brenner[55], E.Brodet[38], P.Bruckman[20], J.M.Brunet[9], B.Buschbeck[57], P.Buschmann[60], M.Calvi[32], T.Camporesi[10], V.Canale[41], F.Carena[10], N.Castro[25], F.Cavallo[6], M.Chapkin[45], Ph.Charpentier[10], P.Checchia[39], R.Chierici[10], P.Chliapnikov[45], J.Chudoba[10], S.U.Chung[10], K.Cieslik[20], P.Collins[10], R.Contri[15], G.Cosme[23], F.Cossutti[52], M.J.Costa[56], D.Crennell[40], J.Cuevas[37], J.D'Hondt[3], T.da Silva[54], W.Da Silva[28], G.Della Ricca[52], A.De Angelis[53], W.De Boer[19], C.De Clercq[3], B.De Lotto[53], N.De Maria[50], A.De Min[39], L.de Paula[54], L.Di Ciaccio[41], A.Di Simone[42], K.Doroba[58], J.Drees[60,10], G.Eigen[5], T.Ekelof[55], M.Ellert[55], M.Elsing[10], M.C.Espirito Santo[25], G.Fanourakis[13], D.Fassouliotis[13,4], M.Feindt[19], J.Fernandez[44], A.Ferrer[56], F.Ferro[15], U.Flagmeyer[60], H.Foeth[10], E.Fokitis[35], F.Fulda-Quenzer[23], J.Fuster[56], M.Gandelman[54], C.Garcia[56], Ph.Gavillet[10], E.Gazis[35], R.Gokieli[10,58], B.Golob[46,48], G.Gomez-Ceballos[44], P.Goncalves[25], E.Graziani[42], G.Grosdidier[23], K.Grzelak[58], J.Guy[40], C.Haag[19], A.Hallgren[55], K.Hamacher[60], K.Hamilton[38], S.Haug[36], F.Hauler[19], V.Hedberg[29], M.Hennecke[19], J.Hoffman[58], S-O.Holmgren[49], P.J.Holt[10], M.A.Houlden[26], J.N.Jackson[26], G.Jarlskog[29], P.Jarry[43], D.Jeans[38], E.K.Johansson[49], P.Jonsson[30], C.Joram[10], L.Jungermann[19], F.Kapusta[28], S.Katsanevas[30], E.Katsoufis[35], G.Kernel[46], B.P.Kersevan[46,48], U.Kerzel[19], B.T.King[26], N.J.Kjaer[10], P.Kluit[34], P.Kokkinias[13], C.Kourkoumelis[4], O.Kouznetsov[18], Z.Krumstein[18], M.Kucharczyk[20], J.Lamsa[1], G.Leder[57], F.Ledroit[16], L.Leinonen[49], R.Leitner[33], J.Lemonne[3], V.Lepeltier†[23], T.Lesiak[20], W.Liebig[60], D.Liko[57], A.Lipniacka[49], J.H.Lopes[54], J.M.Lopez[37], D.Loukas[13], P.Lutz[43], L.Lyons[38], J.MacNaughton[57], A.Malek[60], S.Maltezos[35], F.Mandl[57], J.Marco[44], R.Marco[44], B.Marechal[54], M.Margoni[39], J-C.Marin[10], C.Mariotti[10], A.Markou[13], C.Martinez-Rivero[44], J.Masik[14], N.Mastroyiannopoulos[13], F.Matorras[44], C.Matteuzzi[32], F.Mazzucato[39], M.Mazzucato[39], R.Mc Nulty[26], C.Meroni[31], E.Migliore[50], W.Mitaroff[57], U.Mjoernmark[29], T.Moa[49], M.Moch[19], K.Moenig[10,12], R.Monge[15], J.Montenegro[34], D.Moraes[54], S.Moreno[25], P.Morettini[15], U.Mueller[60], K.Muenich[60], M.Mulders[34], L.Mundim[8], W.Murray[40], B.Muryn[21], G.Myatt[38], T.Myklebust[36], M.Nassiakou[13], F.Navarria[6], K.Nawrocki[58], S.Nemecek[14], R.Nicolaidou[43], M.Nikolenko[18,11], A.Oblakowska-Mucha[21], V.Obraztsov[45], A.Olshevski[18], A.Onofre[25], R.Orava[17], K.Osterberg[17], A.Ouraou[43], A.Oyanguren[56], M.Paganoni[32], S.Paiano[6], J.P.Palacios[26], H.Palka[20], Th.D.Papadopoulou[35], L.Pape[10], C.Parkes[27], F.Parodi[15], U.Parzefall[10], A.Passeri[42], O.Passon[60], L.Peralta[25], V.Perepelitsa[56], A.Perrotta[6], A.Petrolini[15], J.Piedra[44], L.Pieri[42], F.Pierre†[43], M.Pimenta[25], E.Piotto[10], T.Podobnik[46,48], V.Poireau[10], M.E.Pol[7], G.Polok[20], V.Pozdniakov[18], N.Pukhaeva[18], A.Pullia[32], D.Radojicic[38], P.Rebecchi[10], J.Rehn[19], D.Reid[34], R.Reinhardt[60], P.Renton[38], F.Richard[23], J.Ridky[14], M.Rivero[44], D.Rodriguez[44], A.Romero[50], P.Ronchese[39], P.Roudeau[23], T.Rovelli[6], V.Ruhlmann-Kleider[43], D.Ryabtchikov[45], A.Sadovsky[18], L.Salmi[17], J.Salt[56], C.Sander[19], A.Savoy-Navarro[28], U.Schwickerath[10], R.Sekulin[40], M.Siebel[60], A.Sisakian[18], W.Slominski[22], G.Smadja[30], O.Smirnova[29], A.Sokolov[45], A.Sopczak[24], R.Sosnowski[58], T.Spassov[10], M.Stanitzki[19], A.Stocchi[23], J.Strauss[57], B.Stugu[5], M.Szczekowski[58], M.Szeptycka[58], T.Szumlak[21], J.Szwed[22], T.Tabarelli[32], F.Tegenfeldt[55], J.Timmermans[34], L.Tkatchev[18], M.Tobin[26], S.Todorovova[14], B.Tome[25], A.Tonazzo[32], P.Tortosa[56], P.Travnicek[14], D.Treille[10], G.Tristram[9], M.Trochimczuk[58], C.Troncon[31], M-L.Turluer[43], I.A.Tyapkin[18], P.Tyapkin[18], S.Tzamarias[13], V.Uvarov[45], G.Valenti[6], P.Van Dam[34], J.Van Eldik[10], N.van Remortel[2], I.Van Vulpen[10], G.Vegni[31], F.Veloso[25], W.Venus[40], P.Verdier[30], V.Verzi[41], D.Vilanova[43], L.Vitale[52], V.Vrba[14], H.Wahlen[60], A.J.Washbrook[26], C.Weiser[19], D.Wicke[10], J.Wickens[3], G.Wilkinson[38], M.Winter[11], M.Witek[20], O.Yushchenko[45], A.Zalewska[20], P.Zalewski[58], D.Zavrtanik[47], V.Zhuravlov[18], N.I.Zimin[18], A.Zintchenko[18], M.Zupan[13]

[1]Department of Physics and Astronomy, Iowa State University, Ames IA 50011-3160, USA
[2]Physics Department, Universiteit Antwerpen, Universiteitsplein 1, B-2610 Antwerpen, Belgium
[3]IIHE, ULB-VUB, Pleinlaan 2, B-1050 Brussels, Belgium
[4]Physics Laboratory, University of Athens, Solonos Str. 104, GR-10680 Athens, Greece
[5]Department of Physics, University of Bergen, Allégaten 55, NO-5007 Bergen, Norway
[6]Dipartimento di Fisica, Università di Bologna and INFN, Viale C. Berti Pichat 6/2, IT-40127 Bologna, Italy
[7]Centro Brasileiro de Pesquisas Físicas, rua Xavier Sigaud 150, BR-22290 Rio de Janeiro, Brazil
[8]Inst. de Física, Univ. Estadual do Rio de Janeiro, rua São Francisco Xavier 524, Rio de Janeiro, Brazil
[9]Collège de France, Lab. de Physique Corpusculaire, IN2P3-CNRS, FR-75231 Paris Cedex 05, France
[10]CERN, CH-1211 Geneva 23, Switzerland
[11]Institut Pluridisciplinaire Hubert Curien, Université de Strasbourg, IN2P3-CNRS, BP28, FR-67037 Strasbourg Cedex 2, France
[12]Now at DESY-Zeuthen, Platanenallee 6, D-15735 Zeuthen, Germany
[13]Institute of Nuclear Physics, N.C.S.R. Demokritos, P.O. Box 60228, GR-15310 Athens, Greece
[14]FZU, Inst. of Phys. of the C.A.S. High Energy Physics Division, Na Slovance 2, CZ-182 21, Praha 8, Czech Republic
[15]Dipartimento di Fisica, Università di Genova and INFN, Via Dodecaneso 33, IT-16146 Genova, Italy
[16]Institut des Sciences Nucléaires, IN2P3-CNRS, Université de Grenoble 1, FR-38026 Grenoble Cedex, France
[17]Helsinki Institute of Physics and Department of Physical Sciences, P.O. Box 64, FIN-00014 University of Helsinki, Finland
[18]Joint Institute for Nuclear Research, Dubna, Head Post Office, P.O. Box 79, RU-101 000 Moscow, Russian Federation
[19]Institut für Experimentelle Kernphysik, Universität Karlsruhe, Postfach 6980, DE-76128 Karlsruhe, Germany
[20]Institute of Nuclear Physics PAN,Ul. Radzikowskiego 152, PL-31142 Krakow, Poland
[21]Faculty of Physics and Nuclear Techniques, University of Mining and Metallurgy, PL-30055 Krakow, Poland
[22]Institute of Physics, Jagiellonian University, ul. Reymonta 4, 30-059 Krakow, Poland
[23]LAL, Univ Paris-Sud, CNRS/IN2P3, Orsay, France
[24]School of Physics and Chemistry, University of Lancaster, Lancaster LA1 4YB, UK
[25]LIP, IST, FCUL - Av. Elias Garcia, 14-1^{o}, PT-1000 Lisboa Codex, Portugal
[26]Department of Physics, University of Liverpool, P.O. Box 147, Liverpool L69 3BX, UK
[27]Dept. of Physics and Astronomy, Kelvin Building, University of Glasgow, Glasgow G12 8QQ, UK
[28]LPNHE, IN2P3-CNRS, Univ. Paris VI et VII, Tour 33 (RdC), 4 place Jussieu, FR-75252 Paris Cedex 05, France
[29]Department of Physics, University of Lund, Sölvegatan 14, SE-223 63 Lund, Sweden
[30]Université Claude Bernard de Lyon, IPNL, IN2P3-CNRS, FR-69622 Villeurbanne Cedex, France
[31]Dipartimento di Fisica, Università di Milano and INFN-MILANO, Via Celoria 16, IT-20133 Milan, Italy
[32]Dipartimento di Fisica, Univ. di Milano-Bicocca and INFN-MILANO, Piazza della Scienza 3, IT-20126 Milan, Italy
[33]IPNP of MFF, Charles Univ., Areal MFF, V Holesovickach 2, CZ-180 00, Praha 8, Czech Republic
[34]NIKHEF, Postbus 41882, NL-1009 DB Amsterdam, The Netherlands
[35]National Technical University, Physics Department, Zografou Campus, GR-15773 Athens, Greece
[36]Physics Department, University of Oslo, Blindern, NO-0316 Oslo, Norway
[37]Dpto. Fisica, Univ. Oviedo, Avda. Calvo Sotelo s/n, ES-33007 Oviedo, Spain
[38]Department of Physics, University of Oxford, Keble Road, Oxford OX1 3RH, UK
[39]Dipartimento di Fisica, Università di Padova and INFN, Via Marzolo 8, IT-35131 Padua, Italy
[40]Rutherford Appleton Laboratory, Chilton, Didcot OX11 OQX, UK
[41]Dipartimento di Fisica, Università di Roma II and INFN, Tor Vergata, IT-00173 Rome, Italy
[42]Dipartimento di Fisica, Università di Roma III and INFN, Via della Vasca Navale 84, IT-00146 Rome, Italy
[43]DAPNIA/Service de Physique des Particules, CEA-Saclay, FR-91191 Gif-sur-Yvette Cedex, France
[44]Instituto de Fisica de Cantabria (CSIC-UC), Avda. los Castros s/n, ES-39006 Santander, Spain
[45]Inst. for High Energy Physics, Serpukov P.O. Box 35, Protvino, (Moscow Region), Russian Federation
[46]J. Stefan Institute, Jamova 39, SI-1000 Ljubljana, Slovenia
[47]Laboratory for Astroparticle Physics, University of Nova Gorica, Kostanjeviska 16a, SI-5000 Nova Gorica, Slovenia
[48]Department of Physics, University of Ljubljana, SI-1000 Ljubljana, Slovenia
[49]Fysikum, Stockholm University, Box 6730, SE-113 85 Stockholm, Sweden
[50]Dipartimento di Fisica Sperimentale, Università di Torino and INFN, Via P. Giuria 1, IT-10125 Turin, Italy
[51]INFN,Sezione di Torino and Dipartimento di Fisica Teorica, Università di Torino, Via Giuria 1, IT-10125 Turin, Italy
[52]Dipartimento di Fisica, Università di Trieste and INFN, Via A. Valerio 2, IT-34127 Trieste, Italy
[53]Istituto di Fisica, Università di Udine and INFN, IT-33100 Udine, Italy
[54]Univ. Federal do Rio de Janeiro, C.P. 68528 Cidade Univ., Ilha do Fundão BR-21945-970 Rio de Janeiro, Brazil
[55]Department of Radiation Sciences, University of Uppsala, P.O. Box 535, SE-751 21 Uppsala, Sweden
[56]IFIC, Valencia-CSIC, and D.F.A.M.N., U. de Valencia, Avda. Dr. Moliner 50, ES-46100 Burjassot (Valencia), Spain
[57]Institut für Hochenergiephysik, Österr. Akad. d. Wissensch., Nikolsdorfergasse 18, AT-1050 Vienna, Austria
[58]Inst. Nuclear Studies and University of Warsaw, Ul. Hoza 69, PL-00681 Warsaw, Poland
[59]Now at University of Warwick, Coventry CV4 7AL, UK

[60]Fachbereich Physik, University of Wuppertal, Postfach 100 127, DE-42097 Wuppertal, Germany
† deceased

1 Introduction

Single tag $e^+e^- \to e^\pm X$ collisions can be used to determine both the photon [1–5] and electron [6–10] hadronic structure functions. The photon structure function has been studied both theoretically and experimentally for many years [11–23]. Experimental results on the electron structure function (ESF) are presented for the first time in this Letter.

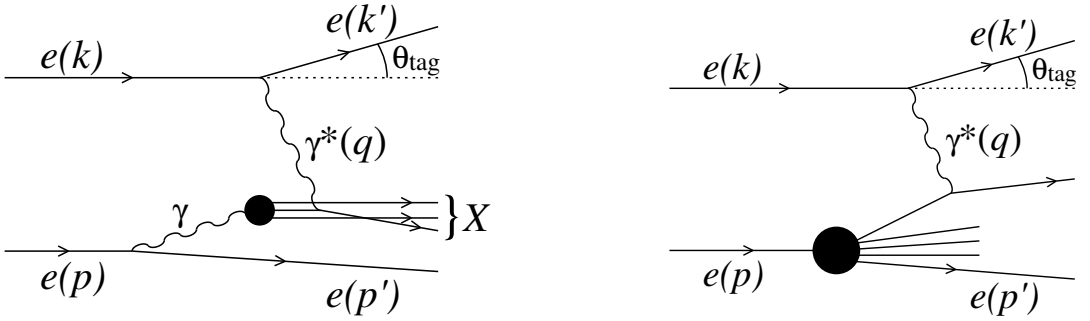

(1a) (1b)

Figure 1: Deep inelastic scattering on a photon target (1a), and on an electron target (1b); p, p', k and k' denote the corresponding four-momenta and q is the four-momentum of the radiated photon.

Although both analyses start from the same set of events the procedures are quite different mainly due to different kinematics. In the photon case (Fig.1a) the spectrum of virtual photons emitted by the (untagged) electron is strongly peaked at small virtualities P^2 (this quantity can be expressed in terms of the untagged electron four-momenta, $P^2 = -(p-p')^2$), approximating the photon to be real. However, non-zero virtuality plays a role [10]. In the electron case (Fig.1b) the photon scatters on a real particle so the problem does not appear. Another difference is the determination of the Bjorken variables x (z) representing the fraction of the struck parton momentum with respect to the photon (electron). In the first case, since the photon momentum is not known, the total hadronic mass W, which cannot be well determined as the majority of hadrons are going in the beam pipe, must be used to determine x,

$$x \cong \frac{Q^2}{Q^2 + W^2} \ , \tag{1}$$

where $Q^2 = -(k-k')^2$ is the negative momentum squared of the deeply virtual (probing) photon. The z variable for the electron is determined directly - as in the classical deep inelastic scattering i.e. from the scattered electron variables only (see below). A certain drawback of the electron structure function is its expected shape: it contains the sharply peaked photon distribution and is dominated by this shape. Hence the same data can be reanalyzed in terms of the electron structure function and the results compared to the usual photon structure function analysis. One can expect that these two independent electron and photon structure functions measurements will help to improve phenomenological parametrizations of the quark content inside the photon and the electron.

The case of the electron structure function is illustrated in Fig.1b. The upper (tagged) electron emits a photon of high virtuality $Q^2 = -q^2$ which scatters off the target electron constituents. The cross-section for such a process under the assumption that $Q^2 \gg P^2$, is:

$$\frac{d^2\sigma(ee \to eX)}{dzdQ^2} = \frac{2\pi\alpha^2}{zQ^4} \left[\left(1 + (1-y)^2\right) F_2^e(z,Q^2) - y^2 F_L^e(z,Q^2) \right] , \tag{2}$$

where

$$y = 1 - (E_{\rm tag}/E)\cos^2(\theta_{\rm tag}/2), \tag{3}$$

with E, $E_{\rm tag}$ and $\theta_{\rm tag}$ being the beam electron initial, final energy and scattering angle, respectively. $F_2^e(z,Q^2)$ and $F_L^e(z,Q^2)$ are the electron structure functions related to the transversal and longitudinal polarization states of the probing photon. The parton momentum fraction, z, is defined in the standard (deep inelastic) way:

$$z = \frac{Q^2}{2pq} = \frac{\sin^2(\theta_{\rm tag}/2)}{E/E_{\rm tag} - \cos^2(\theta_{\rm tag}/2)}\ , \tag{4}$$

and is measured, by means of the tagged electron variables only. The virtuality of the probing photon can be also expressed in terms of E, E_{tag}, θ_{tag} as follows:

$$Q^2 = 4EE_{tag}\sin^2(\theta_{tag}/2). \tag{5}$$

At the leading order, the structure function $F_2^e(z,Q^2)$, which dominates the cross-section at small y, has a simple partonic interpretation:

$$F_2^e(z,Q^2) = z\sum_{i=q,\bar{q}} e_i^2 f_i^e(z,Q^2), \tag{6}$$

where e_i and f_i^e are the i-th quark/anti-quark fractional charge and density.

In e^+e^- experiments the two-photon hadronic cross-section is expressed in terms of two real photon structure functions $F_2^\gamma(x,Q^2)$ and $F_L^\gamma(x,Q^2)$ which leads to the formula analogous to (2)

$$\frac{d^2\sigma(e\gamma\to eX)}{dxdQ^2} = \frac{2\pi\alpha^2}{xQ^4}\left[(1+(1-y_\gamma)^2)F_2^\gamma(x,Q^2) - y_\gamma^2 F_L^\gamma(x,Q^2)\right], \tag{7}$$

where y_γ is the photon energy with respect to the electron energy and F_2^γ, F_L^γ are the photon structure functions related to the transverse and longitudinal polarization states of the probing photon respectively.

Since the photon structure function analysis makes use of the same $\sigma(ee\to eX)$ cross-section, as stated in equation (2), the $\sigma(e\gamma\to eX)$ cross-section must be corrected by a density of photons in the target electron $f_\gamma^e(y_\gamma,P^2)$ (photon flux). The photon flux depends on the momentum transfer squared, P^2, taken at the target photon vertex:

$$f_\gamma^e(y_\gamma,P^2) = \frac{\alpha}{2\pi P^2}\left[\frac{1+(1-y_\gamma^2)}{y_\gamma} - 2y_\gamma\frac{m_e^2}{P^2}\right], \tag{8}$$

where α is the fine structure constant and m_e is the electron mass.

In [6–10] the construction of the electron structure function has been studied together with the Q^2 evolution equations and their asymptotic solutions. This approach has also been compared with the "photon structure function" approach. Although the determinations of the electron and photon structure functions are quite different the functions are simply interrelated:

$$F_{2/L}^e(z,Q^2,P^2_{\rm max}) = \int_z^1 dy_\gamma \int_{P^2_{\rm min}}^{P^2_{\rm max}} dP^2 f_\gamma^e(y_\gamma,P^2)\, F_{2/L}^\gamma(z/y_\gamma,Q^2,P^2), \tag{9}$$

where $P^2_{\rm min} = m_e^2 y_\gamma^2/(1-y_\gamma)$ and P^2_{max} is the maximum value of four-momentum transfer in the lower vertex and it is fixed by the STIC luminometer geometry (see section 2.1) and the anti-tag condition.

P^2 is not measurable for single tag events and, as discussed in detail in [9], the extraction of 'real' photon structure function, F_2^γ, is based on the Weizsäcker-Williams approximation, where P^2 is set to zero in $F_{2/L}^\gamma(x, Q^2, P^2)$. This leads to some underestimation of F_2^γ and the amount of this underestimation depends on the kinematics and geometry of each experiment. This problem is eliminated in the case of electron structure function. Formula (9) enables any existing parametrization of the photon structure function, both real ($P^2 = 0$) and virtual (P^2 dependent), to be tested on the measured electron structure function.

In this paper we report on the measurement of the electron structure function using LEPI and LEPII data. Section 2 describes the selection process of the event sample collected for the analysis and the determination of the detector efficiency. Section 3 presents the measurement of the Electron Structure Function. Conclusions are given in section 4.

2 Experimental procedure

2.1 The DELPHI detector

A detailed description of the DELPHI detector can be found in [24,25] and therefore only a short review of the sub-detectors relevant to the presented analysis is discussed. The DELPHI detector provides 3-dimensional information on curvature and energy deposition with very good spatial resolution as well as identification of leptons and hadrons over most of the solid angle.

The most relevant parts of the setup for the ESF analysis could be divided into two groups. The first one consists of the detectors which are used in the reconstruction of the hadronic final state. They are: the Vertex Detector, the Inner Detector, the Time Projection Chamber (the main DELPHI tracking device) and the Outer Detector. Those devices are operated in the 1.23 T magnetic field parallel to the beam axis. Tracking in the forward (backward) regions is provided by the Forward Chambers. The tracking detectors cover polar angles from 20° to 160° at radii 120 to 2060 mm for the barrel region. The Forward Chambers cover polar angles from 11° to 35° (forward sector) and 145° - 169° (backward sector). Using this subsystem one can reconstruct the charged particle momentum with a resolution $\frac{\sigma(p)}{p} \approx 0.0015 \cdot p$, where p is momentum in GeV. The Hadron calorimeter provides energy measurements of neutral particles.

The second group consists of detectors providing the electromagnetic shower energy measurement. The crucial one is the luminosity calorimeter STIC (Small Angle Tile Calorimeter). The STIC is a lead-scintillator calorimeter formed by two cylindrical detectors placed on both sides of the DELPHI interaction point at a distance of 2200 mm and covers the angular region between 1.7° and 10.5° in polar angle at radii 65 to 420 mm. The STIC energy measurements are used to define the tag condition.

2.2 Event Selection

The analysis has been carried out with the data samples collected by DELPHI at both LEPI and LEPII centre-of-mass energies ranging from 91.2 GeV up to 209.5 GeV and corresponding to integrated luminosities of 72 pb^{-1} at LEPI and 487 pb^{-1} at LEPII. A summary of the used data samples luminosity (along with the number of events selected for each subsample) is given in Table 1.

Table 1: Nominal centre-of-mass energies, integrated luminosities of the used data samples from the LEPII data taking period and the corresponding number of selected events.

Year	$\sqrt{(s)}$	Integrated $L(pb^{-1})$	Number of sel. events
1996	172	10	198
1997	183	53	1001
1998	189	155	3398
1999	196	76	1715
	200	83	1865
	202	40	901
2000	205	70	1842

The most important criterion to select $\gamma\gamma$ events was that one of the two scattered electrons [1] was found in the STIC (tag-condition) whereas the second electron remained undetected (anti-tag condition). Such events are referred to as single-tag events. It was required that the energy deposited by the tagged electron in the STIC had to be greater than $0.65 \cdot E_{beam}$ and no additional energy clusters exceeding $0.25 \cdot E_{beam}$ had been detected in the STIC. The measured energy and angle of the scattered electron allow the squared momentum transfer Q^2 to be determined.

The further step was to select $\gamma\gamma$ induced hadronic final states - with detected charged particles multiplicity greater than 3. Charged particles were defined as reconstructed tracks with momentum above 0.2 GeV, extrapolating to within 4 cm from the primary vertex in the transverse ($R\phi$) plane and within 10 cm along the beam direction (z-axis). The relative uncertainty on the momentum of a charged particle candidate $\frac{\Delta p}{p}$ had to be smaller than 1, its polar angle with respect to the beam axis had to be between 20° and 160° and its measured track length in the TPC greater than 40 cm. To satisfy the trigger condition at least one of the charged particles had to have a momentum larger than 0.7 GeV for LEPI (1.0 GeV for LEPII). The total energy of all charged particles had to be greater than 3 GeV and the minimum of the visible invariant mass of all tracks was fixed at 3 GeV.

The Monte Carlo simulations of e^+e^- annihilation processes with PYTHIA [26–28] and four-fermion processes with EXCALIBUR [29] show that the dominant background contributions come from Z^0 hadronic decays and the two-photon production of $\tau\tau$ pairs. In order to minimize these the following cuts were imposed:

- the vector sum of the transverse momenta of all charged particles, normalised to the total beam energy had to be greater than 0.12 for LEPI (0.14 for LEPII);
- the normalised (like above) sum of the absolute values of the longitudinal momenta of all charged particles (including tagged electron) had to be greater than 0.6;
- the angle between the transverse momenta of the tagged electron and of the charged particles system had to be greater than 120°;
- the maximum of the visible invariant mass was fixed at 40 GeV for LEPI (60 GeV for LEPII data taking).

Among the 21430 events of the LEPI data set (101913 for LEPII) with one high-energy deposit in the STIC calorimeter, 2168 events (10920 for LEPII) passed the above criteria. The total background contribution estimated from the simulation amounted to 111 events for LEPI (1027 for LEPII).

[1] electron is used for both electron and positron.

2.3 Efficiency estimate

In order to evaluate the electron structure function one needs to measure two independent variables, the polar angle θ_{tag} of the scattered (tagged) electron and its energy. Both these quantities are well measured using the STIC luminometer. The measurement of these quantities allows a direct determination of the z and Q^2 variables describing the electron structure function (see formula (4,5)).

The measured cross-sections have been corrected for detector inefficiency computed from a MC generated sample of events passed through the detector simulation program and the selection criteria. As the efficiency computation is model dependent, it is very important to use an event-generator that describes correctly the real data events. In this analysis the TWOGAM [30] event generator together with the JETSET [27] Parton Shower algorithms for the quark and gluon fragmentation have been used. The TWOGAM cross-sections consist of three independent components:

- soft-hadronic part described by the Generalized Vector Dominance Model;
- point-like component, QPM;
- resolved photon interaction, RPC.

The GRV-LO [31] parametrization of the photon structure function was adopted. More details can be found in [30]. To estimate the uncertainty coming from the model we have also used a PYTHIA sample of events. The selection criteria presented in Section 2.2 imposed on real data have also been applied to both simulated samples. For instance, the visible background-subtracted cross-sections for LEPII data as a function of: 1) cosine of the scattered electron angle $\cos(\theta_{tag})$, 2) the probing photon virtuality Q^2, 3) the scattered electron energy E_{tag} and 4) the visible hadronic invariant mass W_{vis} are compared to both simulated samples at the same luminosity (Fig.2). TWOGAM distributions show better agreement with real data cross-sections than those obtained with the PYTHIA event generator. All these discrepancies, both between real data and TWOGAM and real data and PYTHIA have been taken into account in an estimate of the systematic uncertainties. One has to stress that even though the number of events generated by both generators are different the efficiencies do not differ more than about 5 percent.

3 Determination of the Electron Structure Function

The ESF can be extracted as a function of two variables z and Q^2 from formula (2) under the assumption that the longitudinal term F_L^e contribution is negligible which is justified at kinematical range accessible at LEPII energies [32,33],

$$F_2^e(\xi, Q^2) = C \frac{Q^4}{(1+(1-y)^2)} \frac{d^2\sigma(ee \to eX)}{d\xi dQ^2} \ , \tag{10}$$

where $\xi = \log_{10}(z)$ and C is the product of all constant factors.

The measured function $F_2^e(\xi, Q^2)^{meas}$ was corrected in each $\Delta\xi_i \Delta Q_k^2$ bin by the corresponding detector efficiency function $E(\xi, Q^2)$, yielding the reconstructed ESF $F_2^e(\xi, Q^2)^{rec}$. Such a procedure is justified since the migration effect of events generated in any of the (ξ, Q^2) bins to neighbouring bins, after passing the detector simulation, is small. In Fig.3 one can see the smearing caused by the detector for both, the standard photon x-variable Eq.(1) and the standard electron z-variable Eq.(4), for events with fixed value of x=0.1 and z=0.01 generated and passed through the detector simulation

program. Contrary to the narrow z distribution, the x distribution is shifted to higher values and spread over the whole region of x. For that reason the x distribution, related to the photon structure functions, has to be treated in a special way by means of an unfolding procedure. The one-dimensional unfolding requires the knowledge on the theoretical shape of the photon-photon invariant mass distribution in order to convert W_{vis} into the reconstructed one, W_{rec}, whereas the determination of the ESF based on z is not sensitive to that distribution.

The measured Electron Structure Function was averaged over Q^2 in the considered region of the probing photon virtuality leaving only the ξ dependence [2]. The ESF is shown in Figs.4-6 for six Q^2 intervals, $Q^2 \in (4.5, 16)$ GeV^2 for LEPI data as well as $Q^2 \in (16, 20)\,\mathrm{GeV}^2$, $Q^2 \in (20, 30)\,\mathrm{GeV}^2$, $Q^2 \in (30, 50)\,\mathrm{GeV}^2$, $Q^2 \in (50, 80)\,\mathrm{GeV}^2$ and $Q^2 \in (80, 200)$ GeV^2 for LEPII. Fig.4 shows the ESF extracted from LEPI data together with the GRV-LO (lowest-order), GRV-HO (higher-order) [31] and SaS [34] photon predictions. In order to calculate F_2^e we convolute F_2^γ from the parametrization with the photon flux according to equation (9). For LEPII data, Figs.5-6, we plot the latest predictions of some NLO resolved photon parametrizations, GRV-HO [35,36], AFG [37], CJK-HO [38], and SAL [39]. For AFG and SAL we use F_2^γ provided by the authors, while for GRV and CJK we calculate F_2^γ from PDFs using phenomenological treatment of massive quarks described in [39]. Due to a non-zero minimum polar tagging angle the untagged electron may still radiate a virtual photon up to $P^2 \approx 4$ GeV^2 at LEPI and $P^2 \approx 19$ GeV^2 at LEPII. As a consequence the effects of the target photon virtuality can be non-negligible. Lacking the P^2 dependent virtual photon parametrizations we use predictions based on the real photon approximation. The target virtuality P^2 is taken into account only in the photon flux given in equation (8). In Fig.7 SaS model predictions for two virtualities of the target photon $P^2 = 0.5$ GeV^2 and $P^2 = 4.0$ GeV^2 are shown. A similar difference is observed for other parametrizations at LEPII energies [9].

Since the radiative corrections (important for LEPII) were not incorporated into the theoretical predictions the experimental data (Figs.4-6) have been corrected. The corrections have been calculated using the TWOGAM generator that allows to produce both radiative corrected and un-corrected data. Two large samples have been generated and processed by the full detector simulation framework and the correction factors extracted. It has been shown that the maximum value of the radiative correction is about 1.5% and 7% for LEPI and LEPII respectively.

For LEPI the data points follow predictions of the earlier GRV-HO, GRV-LO and SaS models. For LEPII energies in the middle range of $Q^2 \in (20 \sim 50)$ GeV^2 and for smaller value of ξ there is a general tendency for all parametrizations to lie slightly above the data points. This effect is more clear for the AFG and CJK-HO parametrizations. The measurements of the ESF for LEPI and LEPII together with statistical and systematic uncertainties are presented in Table 2 and 3.

The statistical uncertainties in each bin of the considered event distribution have been calculated according to the Poisson law and then propagated to the final distributions. The systematic uncertainty has the following contributions:

- uncertainties due to the STIC detector bias (corresponding to the absolute calibration error) of the electron energy ($\frac{\sigma_E}{E} = 0.13\%$) and scattering angle ($\sigma_\theta = 0.45$ mrad) of the tagged electron measurements. To estimate this contribution the energy E_{tag} and angle θ_{tag} of each tagged electron have been varied by the calibration uncertainties successively. The ESF has been recomputed each time and the systematical uncertainty has been taken as the maximum deviation between ESF values.

[2] The phase space dependence of Q^2 versus the ξ and E variables translates into unequal intervals of ξ in Figs.4-6

- uncertainty due to binning variation. This has been estimated evaluating the ESF for three different sets of binnings.
- the efficiencies resulting from TWOGAM and PYTHIA models do not differ more than about 5% and were incorporated to the systematic uncertainties.

Table 2: Results of the measurements of the electron structure function for LEPI energies.

Q^2 GeV^2	$\langle Q^2 \rangle$	$-\xi$	$F_2^e(\xi)/\alpha^2$	σ_{stat}	σ_{syst}	σ_{total}
(4.5 – 16)	9.02	0.80 – 1.15	1.30	± 0.29	$^{+0.74}_{-0.69}$	$^{+0.79}_{-0.74}$
		1.15 – 1.50	2.71	± 0.36	$^{+0.64}_{-0.54}$	$^{+0.73}_{-0.65}$
		1.50 – 1.85	3.96	± 0.41	$^{+0.56}_{-0.53}$	$^{+0.69}_{-0.67}$
		1.85 – 2.20	5.62	± 0.44	$^{+0.44}_{-0.48}$	$^{+0.62}_{-0.65}$

Table 3: Results of the measurements of the electron structure function for LEPII energies.

Q^2 GeV^2	$\langle Q^2 \rangle$	$-\xi$	$F_2^e(\xi)/\alpha^2$	σ_{stat}	σ_{syst}	σ_{total}
(16 – 20)	17.3	2.30 – 2.43	8.73	±0.92	$^{+0.47}_{-0.42}$	$^{+1.03}_{-1.01}$
		2.43 – 2.56	12.64	±0.50	$^{+0.47}_{-0.34}$	$^{+0.68}_{-0.61}$
		2.56 – 2.69	12.05	±0.49	$^{+0.46}_{-0.30}$	$^{+0.67}_{-0.57}$
		2.69 – 2.82	14.43	±0.54	$^{+0.61}_{-0.66}$	$^{+0.82}_{-0.85}$
(20 – 30)	24.5	0.80 – 1.10	3.71	±0.31	$^{+0.31}_{-0.40}$	$^{+0.44}_{-0.51}$
		1.10 – 1.40	4.73	±0.20	$^{+0.25}_{-0.22}$	$^{+0.32}_{-0.30}$
		1.40 – 1.70	6.27	±0.21	$^{+0.33}_{-0.22}$	$^{+0.39}_{-0.30}$
		1.70 – 2.00	7.82	±0.26	$^{+0.19}_{-0.23}$	$^{+0.32}_{-0.34}$
		2.00 – 2.30	10.06	±0.30	$^{+0.13}_{-0.29}$	$^{+0.33}_{-0.42}$
		2.30 – 2.60	11.63	±0.37	$^{+0.20}_{-0.26}$	$^{+0.42}_{-0.45}$
(30 – 50)	38.5	0.66 – 0.98	3.93	±0.40	$^{+0.41}_{-0.33}$	$^{+0.57}_{-0.51}$
		0.98 – 1.30	5.51	±0.35	$^{+0.31}_{-0.25}$	$^{+0.47}_{-0.43}$
		1.30 – 1.62	6.82	±0.40	$^{+0.24}_{-0.23}$	$^{+0.47}_{-0.46}$
		1.62 – 1.94	9.18	±0.48	$^{+0.32}_{-0.19}$	$^{+0.58}_{-0.52}$
		1.94 – 2.26	11.58	±0.61	$^{+0.24}_{-0.41}$	$^{+0.66}_{-0.73}$
(50 – 80)	62.4	0.60 – 0.90	2.18	±0.50	$^{+0.33}_{-0.54}$	$^{+0.60}_{-0.74}$
		0.90 – 1.20	5.44	±0.47	$^{+0.60}_{-0.49}$	$^{+0.76}_{-0.68}$
		1.20 – 1.50	7.20	±0.45	$^{+0.36}_{-0.43}$	$^{+0.58}_{-0.62}$
		1.50 – 1.80	8.95	±0.44	$^{+0.54}_{-0.51}$	$^{+0.69}_{-0.67}$
		1.80 – 2.10	12.24	±0.38	$^{+0.64}_{-0.33}$	$^{+0.74}_{-0.50}$
(80 – 200)	130.2	1. – 1.5	7.84	±0.71	$^{+1.53}_{-1.56}$	$^{+1.69}_{-1.71}$
		1.5 – 2.0	11.84	±0.63	$^{+1.19}_{-1.37}$	$^{+1.35}_{-1.51}$

4 Conclusions

The hadronic part of the electron structure function has been measured and has been found to agree with the predictions of the GRV-HO, SaS, SAL05 models. For lower values of the probing photon virtuality a discrepancy between the data and AFG and CJK-HO model predictions exists.

The proposed method, based on directly measured quantities, is simpler than the photon structure analysis as it does not use the unfolding procedure.

It allows the virtuality of the probed photon to be taken into account correctly. It is shown that the migration of events between z-bins (electron) is much smaller than between x-bins (photon). The statistical uncertainties are well understood since in each bin of the measured ESF they directly reflect a Poisson error unlike the photon analysis where the statistical uncertainties have to be propagated through the unfolding procedure. The inclusion of the photon virtuality is important - the difference between the two SaS parametrizations, with and without the P^2 dependence are of the same order as between SaS and GRV-LO, both P^2 independent.

Acknowledgements

We are greatly indebted to our technical collaborators, to the members of the CERN-SL Division for the excellent performance of the LEP collider, and to the funding agencies for their support in building and operating the DELPHI detector.
We acknowledge in particular the support of
Austrian Federal Ministry of Education, Science and Culture, GZ 616.364/2-III/2a/98,
FNRS–FWO, Flanders Institute to encourage scientific and technological research in the industry (IWT) and Belgian Federal Office for Scientific, Technical and Cultural affairs (OSTC), Belgium,
FINEP, CNPq, CAPES, FUJB and FAPERJ, Brazil,
Ministry of Education of the Czech Republic, project LC527,
Academy of Sciences of the Czech Republic, project AV0Z10100502,
Commission of the European Communities (DG XII),
Direction des Sciences de la Matière, CEA, France,
Bundesministerium für Bildung, Wissenschaft, Forschung und Technologie, Germany,
General Secretariat for Research and Technology, Greece,
National Science Foundation (NWO) and Foundation for Research on Matter (FOM), The Netherlands,
Norwegian Research Council,
State Committee for Scientific Research, Poland, SPUB-M/CERN/PO3/DZ296/2000, SPUB-M/CERN/PO3/DZ297/2000, 2P03B 104 19 and 2P03B 69 23(2002-2004),
FCT - Fundação para a Ciência e Tecnologia, Portugal,
Vedecka grantova agentura MS SR, Slovakia, Nr. 95/5195/134,
Ministry of Science and Technology of the Republic of Slovenia,
CICYT, Spain, AEN99-0950 and AEN99-0761,
The Swedish Research Council,
The Science and Technology Facilities Council, UK,
Department of Energy, USA, DE-FG02-01ER41155,
EEC RTN contract HPRN-CT-00292-2002.

References

[1] E. Witten, Nucl. Phys. **B120** (1977) 189.
[2] C.H. Llewellyn Smith, Phys. Lett. **B79** (1978) 83.
[3] R.J. DeWitt et al., Phys. Rev. **D19** (1979) 2046; Erratum ibid **D20** (1979) 1751.
[4] T.F. Walsh and P. Zerwas, Phys. Lett. **B44** (1973) 195.
[5] R.L. Kingsley, Nucl. Phys. **B60** (1973) 45.
[6] W. Słomiński and J. Szwed, Phys. Lett. **B387** (1996) 861.
[7] W. Słomiński and J. Szwed, Acta Phys. Polon. **B27** (1996)1887.
[8] W. Słomiński and J. Szwed, Acta Phys. Polon. **B28** (1997) 1493.
[9] W. Słomiński and J. Szwed, Eur. Phys. J. **C22** (2001) 123.
[10] W. Słomiński, Acta Phys. Polon. **B30** (1999) 369.
[11] H.J. Behrend et al., (CELLO Collaboration), Phys. Lett. **B126** (1983) 391.
[12] Ch. Berger et al., (PLUTO Collaboration), Phys. Lett. **B142** (1984) 111.
[13] W. Bartel et al., (JADE Collaboration), Zeit. f. Phys. **C24** (1984) 231.
[14] M. Althoff et al., (TASSO Collaboration), Zeit. f. Phys. **C31** (1986) 527.
[15] H. Aihara et al., (TPC/2γ Collaboration), Zeit. f. Phys. **C34** (1987) 1.
[16] T. Sasaki et al., (AMY Collaboration), Phys. Lett. **B252** (1990) 491.
[17] R. Akers et al., (OPAL Collaboration), Zeit. f. Phys. **C61** (1994) 199.
[18] S.K. Sahu et al., (AMY Collaboration), Phys. Lett. **B346** (1995) 208.
[19] P. Abreu et al., (DELPHI Collaboration), Zeit. f. Phys. **C69** (1996) 223.
[20] K. Ackerstaff et al., (OPAL Collaboration), Zeit. f. Phys. **C74** (1997) 33.
[21] M. Acciarri et al., (L3 Collaboration), Phys. Lett. **B436** (1998) 403.
[22] M. Acciarri et al., (L3 Collaboration), Phys. Lett. **B447** (1999)147.
[23] R. Barate et al. (ALEPH Collaboration), Phys. Lett. **B458** (1999) 152.
[24] P. Aarnio et al., (DELPHI Collaboration), Nucl. Instr. and Meth. **A303** (1991) 233.
[25] P. Abreu et al., (DELPHI Collaboration), Nucl. Instr. and Meth. **A378** (1996) 57.
[26] T. Sjöstrand, Comp. Phys. Comm. **82** (1994) 74.
[27] T. Sjöstrand, L. Lönnblad, S. Mrenna and P. Skands, *PYTHIA6.3 Physics and Manual*, LU TP 03-38, hep-ph/0308153.
[28] P. Aurenche et al., in *gamma − gamma Physics*, 'Physics at LEP2', CERN 96-01 **Vol.1** (1996) 291.
[29] F.A. Berends, R. Pittau and R. Kleiss, Comp. Phys. Comm. **85** (1995) 437.
[30] T. Alderweireld et al., in *Reports of the Working Groups on Precision Calculations for LEP2 Physics*, eds. S. Jadach, G. Passarino and R. Pittau, CERN 2000-009 (2000) 219.
[31] M. Glück, E. Reya and A. Vogt, Eur. Phys. J. **C5** (1998) 461.
[32] R.Nisius, *Experimental Results on Two-Photon Physics from LEP*, [hep-ex/9909023].
[33] R.Nisius, *Hadronic structure function of the photon measured at LEP*, [hep-ex/0006032].
[34] G. A. Schuler and T. Sjöstrand, Phys. Lett. **B376** (1996) 193.
[35] M. Gluck, E. Reya, A. Vogt, Phys. Rev. **D45** (1992) 3986.
[36] M. Gluck, E. Reya, A. Vogt, Phys. Rev. **D46** (1992) 1973.
[37] P. Aurenche, M. Fontannaz, J.Ph. Guillet, Eur. Phys. J. **C44** (2005) 395 [hep-ph/0503259].
[38] F. Cornet, P. Jankowski and M. Krawczyk, Phys. Rev. **D70** (2004) 093004.
[39] W. Slominski, H. Abramowicz and A. Levy, Eur. Phys. J. **C45** (2006) 633.

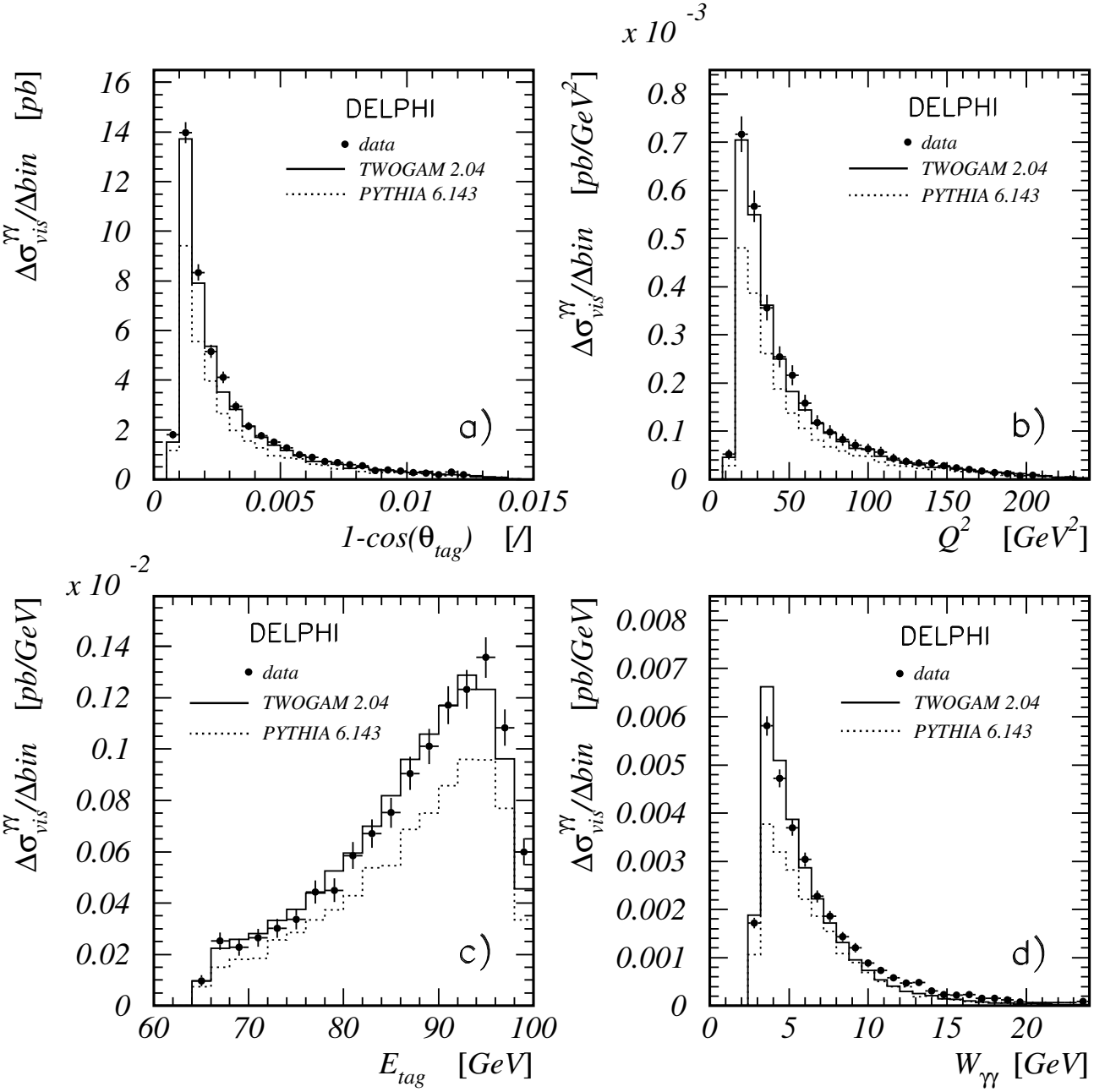

Figure 2: Differential visible cross-sections (at LEPII energies) as a function of (a) cosine of the scattered electron angle θ_{tag}, (b) probing photon virtuality Q^2, (c) energy of scattered electron E_{tag}, (d) visible hadronic invariant mass, for real data (points with error bars) and simulation (histograms).

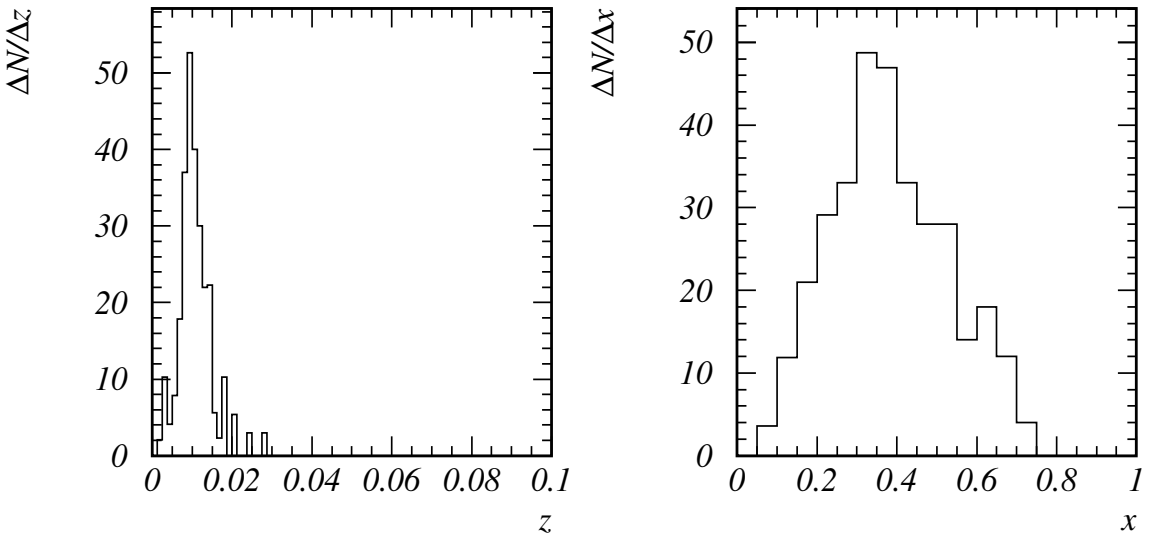

Figure 3: The detector simulated z and x distributions obtained from the sample generated at z=0.01 and x=0.1 (LEPII) and for $Q^2 \in (20, 30)$ GeV^2

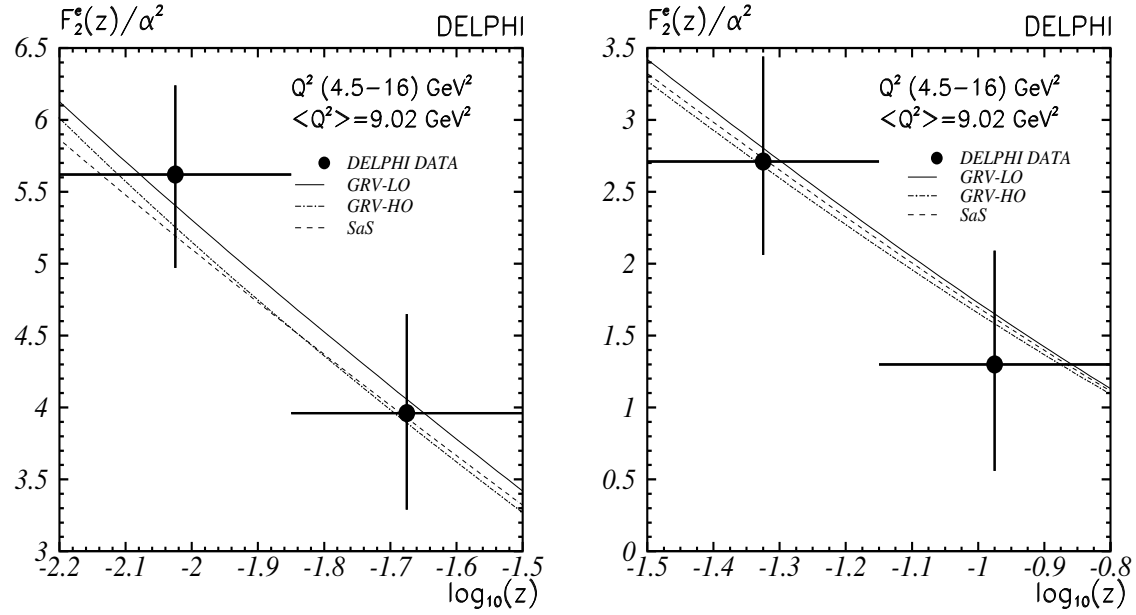

(a) (b)

Figure 4: LEPI data. The electron structure function (ESF) measured for $Q^2 \in (4.5, 16)$ GeV^2. For better separation of the presented models the allowed interval of ξ variable is split and shown separately in Fig.4a and Fig.4b. For each bin the total uncertainty is plotted (the data is corrected for the absence of radiation in the theoretical prediction).

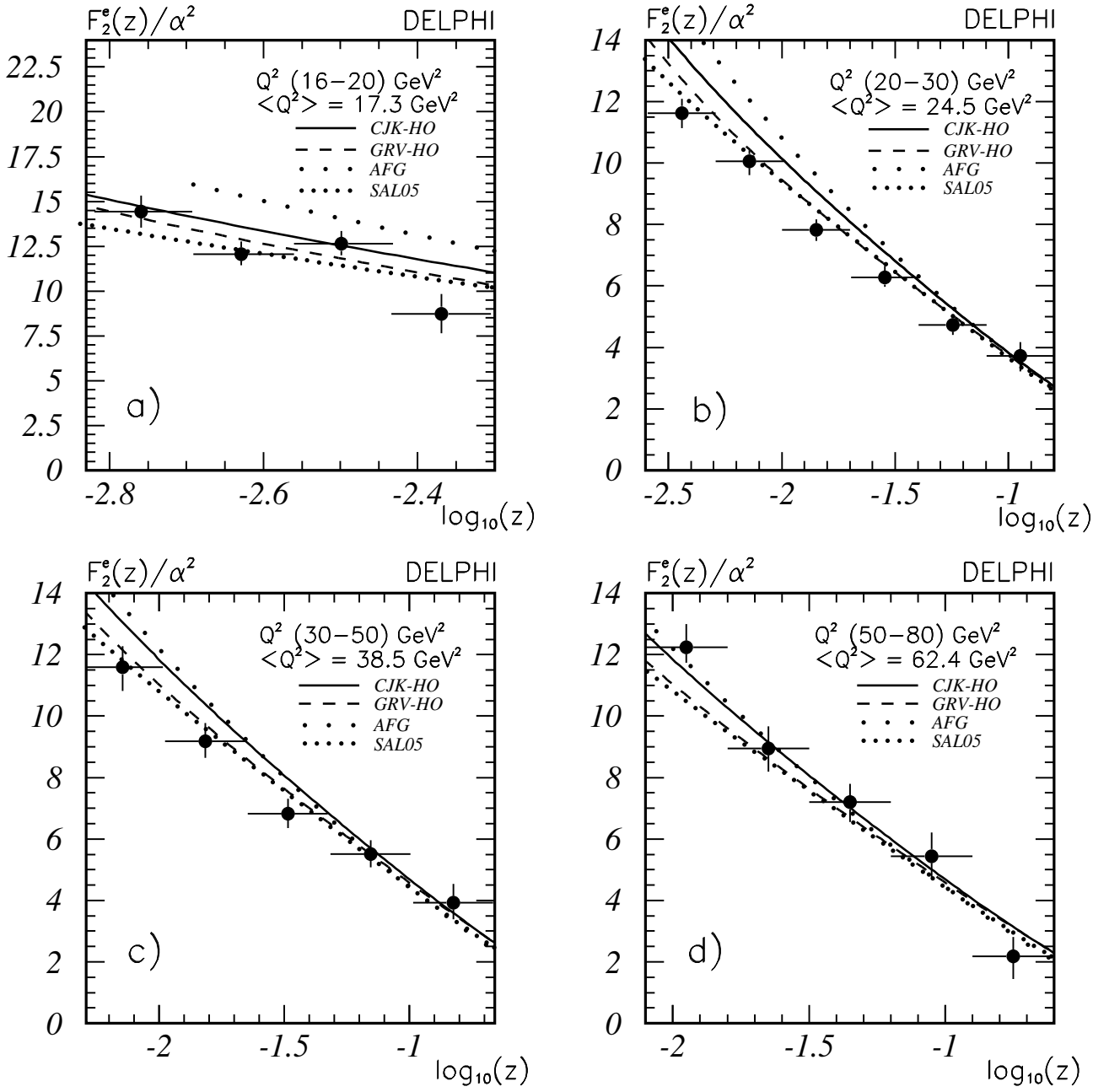

Figure 5: LEPII data. The ESF measured for (a) $Q^2 \in (16, 20)$ GeV^2, (b) $Q^2 \in (20, 30)$ GeV^2, (c) $Q^2 \in (30, 50)$ GeV^2, (d) $Q^2 \in (50, 80)$ GeV^2. For each bin the total uncertainty is plotted (the data is corrected for the absence of radiation in the theoretical prediction).

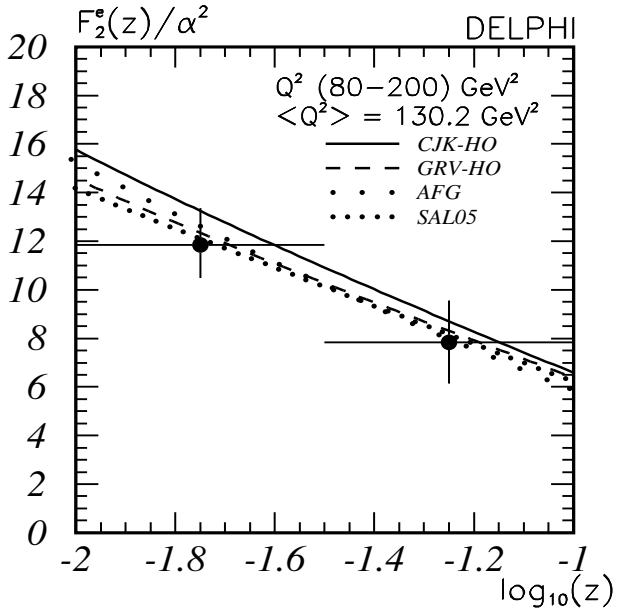

Figure 6: LEPII data. The ESF measured for $Q^2 \in (80, 200)\,\mathrm{GeV}^2$. For each bin the total uncertainty is plotted (the data is corrected for the absence of radiation in the theoretical prediction).

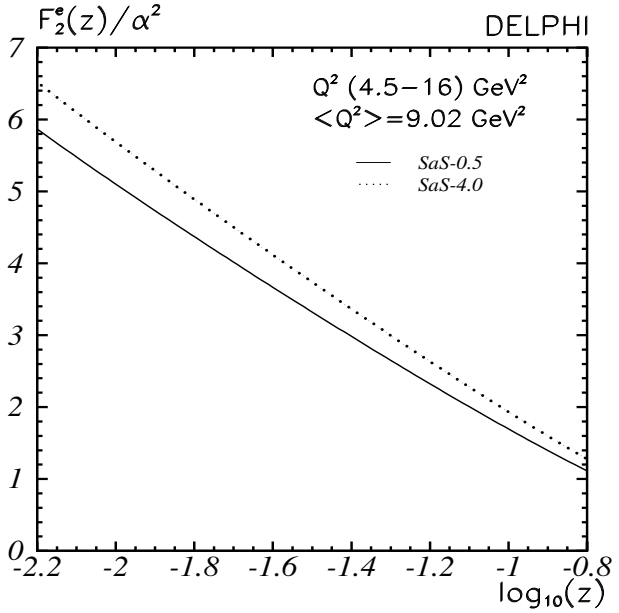

Figure 7: SaS model prediction for two different virtualities of the target photon at LEPI energies. Continuous line corresponds to $P^2 = 0.5$ GeV^2 whereas dotted line corresponds to $P^2 = 4.0$ GeV^2